A Regularized Source Current Reconstruction Method for Reactive Near Field to Far Field Transformation

M. Bod, R. Sarraf-Shirazi, GH. Moradi, and A. Jafargholi

Department of Electrical Engineering
Amirkabir University of Technology, Tehran, Iran
(mbod, sarraf, ghmoradi, amirajafargholi)@aut.ac.ir

Abstract ─ The source current reconstruction method (SRM) is based on reconstructing equivalent current from the known electric field and can be used as a method of near field to far field transformation. In this paper for the first time the reactive near field (RNF) to far field (FF) transformation based on SRM is carefully studied. It is shown that in the RNF region, the singular values of the SRM transformation matrix can magnify the evanescent modes of RNF region and unstable the SRM iterative solvers. Therefore, in this paper for RNF/FF transformation a regularized SRM is proposed and the equivalent magnetic current of an antenna under test is reconstructed from the Tikhonov SRM equation. The regularization parameter of the Tikhonov equation is determined by the L-curve method. The effect of near field distance and noise on the accuracy of far field transformation of the proposed algorithm are studied in two different antenna simulations. It is shown that in all cases in the RNF region a regularized SRM have more stable behavior and more accurate results.

Index Terms ─ Reactive near field, regularization, source current reconstruction, Tikhonov inverse problem.

I. INTRODUCTION

One of the important parameters to characterize the antenna performance is its far field radiation pattern which is measured in an anechoic chamber. In practice, due to size limitation, it is not always possible to measure the far field radiation pattern of the antenna under test (AUT). Therefore, the near field radiation pattern of the AUT is measured and the far field radiation pattern is reconstructed by means of Near Field (NF) to Far Field (FF) transformation [1].

In recent years, many different techniques for NF/FF transformation are developed [1]-[10]. The earliest works are based on the wave mode expansion, in which the measured near field data are used to determine the wave mode coefficients of the AUT [1], [2]. By finding theses wave mode coefficients, it is possible to determine the antenna radiation pattern at any desired distance. However, in these techniques, the spatial sampling rate should satisfy Nyquist criterion and reducing the number of sampling points from that criterion can deteriorate the transformation procedure. Furthermore, the modal techniques are limited to canonical acquisition surfaces (planar, cylindrical or spherical measurements) [3].

Recently, another NF/FF transformation technique, called the sources reconstruction method (SRM), has been proposed [3]-[12]. In this technique by using an equivalence principle, the equivalent currents at the antenna aperture can be reconstructed from the known NF data. By reconstructing the equivalent current at the antenna aperture it is possible to determine the radiation pattern of the AUT at any desired distance.

SRM is, in fact, an inverse radiation problem which is based on an electric field integral equation and is solved by the inverse method of moment techniques [8]. In comparison to the modal methods, SRM is more accurate, more stable and more robust but have a high computational cost associated to the solving of complex integral equations [3]. Furthermore, SRM is based on the full wave equations which are valid in all of the space around the AUT, while modal expansion based NF/FF transformation can be applied outside the minimum sphere enclosing AUT [3].

Until recently, the NF/FF transformation are mostly done with data that measured in the radiative near field region [13]. In fact, unavoidable coupling, reflection, and interferences between the AUT and typical electromagnetic field probes enforce the measurement to be done at distance more than one wavelength from the AUT aperture [13]. With the development of optic sensors and equipment, the reactive near field (RNF) measurement is also possible [13]-[15]. With such progressions in the measurement systems, a method for RNF/FF transformation can drastically reduce the dimensions of test facilities and test costs and increase measurement speeds. However, up to the authors' knowledge, the RNF/FF transformation are not studied well until know.

A brief report about the very near field to far field transformation with the modal techniques can be found in [14]. An accurate RNF/FF transformation is obtained

in this paper by the field sampling strategy that the authors have proposed. In fact, in this paper, the field sampling positions have been optimized for each antenna in a way that creates a transformation matrix with the most convenient singular value. This will reduce the effects of evanescent modes of RNF region as shown in this paper.

A RNF/FF transformation based on SRM technique is reported in [12]. In this paper, it has been shown that the field transformation error of the conventional SRM is increased drastically in the RNF region. Therefore, a dual equation formulation for SRM technique has been proposed. One can be shown that the proposed formulation of SRM technique can noticeably improve the condition number of field transformation matrix and therefore reduce the effects of evanescent modes but this formulation has very high computational cost.

In this paper, the effect of RNF data on the SRM field transformation is completely studied. It is shown that if the singular values of the SRM field transformation matrix are not treated well, the evanescent modes of the RNF region will create instability in the FF transformation. Therefore, in order to reconstruct the FF radiation from the RNF data, a regularized SRM is proposed in the paper. The necessity of regularization for RNF/FF applications are demonstrated both analytically and experimentally. The effect of near field distance and noise on the accuracy of the proposed regularized SRM are studied in two different antenna simulations. It is shown that in all cases, in the RNF region the regularized SRM have more stable and more accurate results.

II. DESCRIPTION OF THE METHOD

A. Source current reconstruction method

The SRM is based on the electromagnetic equivalence principle which allows one to establish an equivalent problem of an AUT radiation by using equivalent electric and magnetic currents [8]. According to this principle, the radiated fields outside the domain containing the equivalent currents are the same in both the original and the equivalent problem. This basic idea is used in the SRM to develop a set of integral equations in which the known electric field is related to the radiation of equivalent current at the AUT aperture.

SRM integral equation can be used to reconstruct both equivalent electric and magnetic currents [8]. However, in the field transformation applications for the simplification of equations, one can assume that a half space perfect electric conductor is placed at the AUT aperture in the xy-plane and reconstruct only an equivalent magnetic current by the following integral equation [4]:

$$\overline{E}(\overline{r}) = -\frac{1}{4\pi} \int_{S'} \overline{M}_{eq}(\overline{r'}) \times \nabla' G_M(\overline{r},\overline{r'}) \ ds', \qquad (1)$$

in which $E(r)$ is the known electric field at the observation point r, M_{eq} is the equivalent magnetic

current at the antenna aperture and G_M is the appropriate dyadic Green function relating the magnetic current and fields in free space.

This integral equation should be discretized and solved via standard method of moments (MOM). For this purpose, the antenna aperture should be meshed with triangular facets as shown in Fig. 1, and the equivalent magnetic current M_{eq} is approximated by a finite sum of Rao-Wilton-Gilson (RWG) subdomain basis functions as follows [9]:

$$\vec{M}_{eq}(\vec{r'}) = \sum_{n=1}^{N} I_{M_n} \cdot \vec{f}_n(\vec{r'}), \qquad (2)$$

in which I_M is the unknown coefficient that should be determined by the method of moment and $\overrightarrow{f_n}(\overrightarrow{r'})$ are the well-known RWG basis functions defined at each triangular facets as shown in Fig. 2 [9].
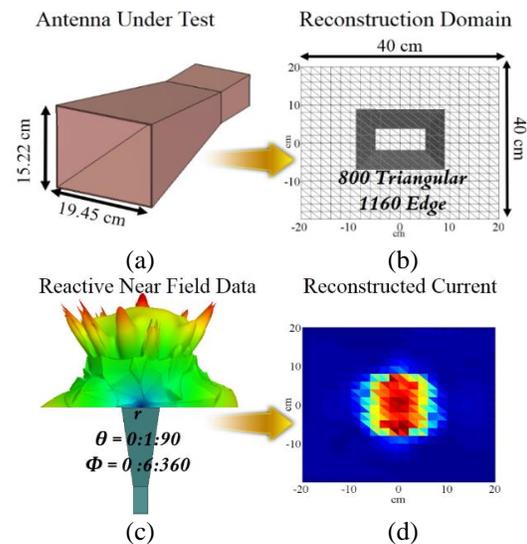
Fig. 1. Source current reconstruction method elements. (a) A horn antenna is selected as an AUT, (b) the RWG facets at the horn antenna aperture, (c) the hemisphere acquisition of reactive near field with λ/2 radius from the antenna aperture, and (d) the reconstructed equivalent magnetic current at the antenna aperture.
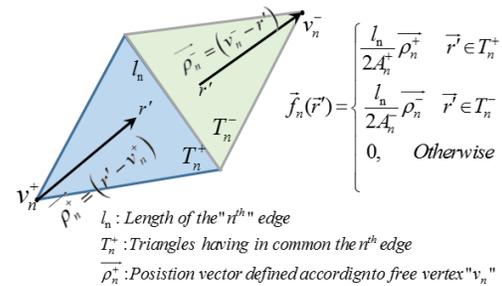
Fig. 2. RWG basis function definition on the triangular facets.

By adding a set of known electric fields at different positions in Equation (1) and using Equation (2), a matrix equation can be constructed as follows:

$$\begin{bmatrix} H_{\theta,I_{M_n}} \\ H_{\phi,I_{M_n}} \end{bmatrix}_{2m \times n} \times \begin{bmatrix} I_{M_n} \end{bmatrix}_{n \times 1} = \begin{bmatrix} E_\theta \\ E_\phi \end{bmatrix}_{2m \times 1}, \qquad (3)$$

where m is the number of measured electric field points, n is the number of unknown coefficients (total edges in RWG basis function) and H is the discretized impedance matrix which has $2 \times m$ column and n rows.

The system of Equations (3) is overdetermined because the number of known field is greater than unknown coefficients. Therefore, Equation (3) should be solved by a least square solver which minimize the following equation:

$$I_M = \arg\min_{I_M} \left\{ \| E - H \times I_M \|_2^2 \right\}. \qquad (4)$$

This least square equation can be solved by the singular value decomposition (SVD) method [5]. In this method, the impedance matrix H is expanded as $H \approx \hat{U}\Sigma\hat{V}^*$ in which matrix $\hat{U}$ contains the left singular vector $\hat{u}_i$, the matrix $\hat{V}$ contains the right singular vector $\hat{v}_i$ and the diagonal matrix Σ contains the singular values σ_i of the impedance matrix H. With this decomposition, the solution of (4) can be considered as follows [16]:

$$I_M = H^\dagger \times E.$$
$$I_M = \left(\sum_{i=1}^{n} \frac{\hat{u}_i^* E}{\sigma_i} \hat{v}_i \right), \qquad (5)$$

where $H^\dagger$ is called the pseudo inverse of matrix H. It should be mentioned that in the applications where a large amount of data is involved in the system of Equations (4), iterative solvers like conjugate gradient (CG), least square QR (LSQR) and etc. is preferred [8].

Once the equivalent magnetic currents are obtained, the final step is to use these currents in the forward radiation problem and find the radiation fields at any desired distance.

B. The regularized SRM

As is shown in the previous section, SRM is an inverse source problem in which the equivalent currents are determined from the known electric field data. Like all other inverse problems, SRM is inherently an ill-posed problem, which means that a solution is very sensitive to small errors and noise.

In order to minimize the effect of measurement errors and noise, a regularized SRM can be applied in which the currents are reconstructed by the Tikhonov Regularization Technique (TRT). It is already shown that the TRT results are more stable in the presence of any type of noise signals [6]. In the TRT, the minimization Equation (4) is replaced by the following equation [6]:

$$I_{reg} = \arg\min_{I_M} \left\{ \| E_{noisy} - H \times I_M \|_2^2 + \Gamma^2 \| I_M \|_2^2 \right\}, \qquad (6)$$

in which E_{noisy} is the measured electric field in the presence of noise and Γ is a regularization parameter. Similar to (5), the solution of Equation (6) can be written as follows [16]:

$$I_{reg} = H^\# \times E_{noisy}.$$
$$I_{reg} = \sum_{i=1}^{n} \left(\frac{\sigma_i \hat{u}_i^* E_{noisy}}{\sigma_i^2 + \Gamma^2} \right) \hat{v}_i, \qquad (7)$$

where $H^\#$ is the pseudo inverse of the regularized Equation (6).

From Equation (7), it is obvious that by adding a regularization parameter to the singular values of H, the effect of perturbation error and noise is reduced. Therefore, the regularized solutions are more stable in the presence of noise. It is also can be understood that if the measurement is noiseless no regularization is needed $(H^\dagger = H^\#)$.

As described before, in this paper we want to investigate the effectiveness of noiseless SRM in the RNF/FF transformation. To evaluate the SRM accuracy, a RNF/FF error can be defined as follows [11]:

$$\varepsilon_{FF} = \frac{\| E_{FF} - E_{SRM-FF} \|_2^2}{\| E_{FF} \|_2^2}, \qquad (8)$$

in which E_{FF} is the reference FF data of the AUT and E_{SRM-FF} is the obtained FF radiation by the SRM equations. The numerator of this equation can be expanded based on the known reactive near field data E_{RN} as follows:

$$Num(\varepsilon_{FF}) = \| E_{FF} - H' \times M_{eq} \|_2^2 = \| E_{FF} - H' \times (H^\dagger \times E_{RNF}) \|_2^2, \qquad (9)$$

in which H' is the impedance matrix of the forward problem which transform the equivalent currents to the FF radiation fields.

As is known in the RNF region, the electric field E_{RN} is composed of evanescent and non-evanescent modes and can be written as follows:

$$E_{RNF} = E_{Non-Ev.} + E_{Ev.} \qquad (10)$$

If this equation is used in the FF transformation error of Equation (9) and the $H^\dagger$ matrix is replaced by its SVD, the following equation is obtained:

$$Num(\varepsilon_{FF}) = \left\| E_{FF} - H' \times \sum_{i=1}^{n} \left(\frac{u_i^* E_{Ev.}}{\sigma_i} \right) v_i - H' \times \sum_{i=1}^{n} \left(\frac{u_i^* E_{Non-Ev.}}{\sigma_i} \right) v_i \right\|_2^2. \qquad (11)$$

In this equation the forward radiation matrix H' is ideally try to filter all of the evanescent terms of electric field and amplify the non-evanescent terms in order to create the stable far field radiation. However if the singular values of $H^\dagger(\sigma_i)$ are not treated well, mathematically they can magnify the non-desirable evanescent modes in Equation (11) and makes the far field radiation unstable. This important point is neglected

in the SRM papers until now [3]-[12]. This instability in the far field transformation error in Equation (11) can be resolved by replacing $H^\dagger$ with $H^\sharp$ as follows:

$$Num(\varepsilon_{FF}) = \left\| E_{FF} - H' \times H^\sharp \times E_{Ev.} - H' \times H^\sharp \times E_{Non-Ev.} \right\|_2^2,$$

$$= \left\| E_{FF} - H' \times \sum_{i=1}^{n} \left(\frac{\sigma_i u_i^* E_{Ev.}}{\sigma_i^2 + \Gamma^2} \right) v_i - H' \times \sum_{i=1}^{n} \left(\frac{\sigma_i u_i^* E_{Non-Ev.}}{\sigma_i^2 + \Gamma^2} \right) v_i \right\|_2^2 . \quad (12)$$

It should be emphasized that in the above equations it is assumed that all the measurements are noiseless, however, because of a large amount of evanescent modes, only a regularized SRM have a stable behavior in the RNF/FF transformation. In (12) the term $H' \times H^\sharp \times E_{Ev.}$ can be defined as a regularized perturbation error in the noiseless RNF/FF transformation.

C. Determination of the regularization parameter

Once the necessity of regularization in the RNF/FF transformation is shown, the next step is to introduce a method for determining the regularization parameter, Γ, in the Equation (6). In the open literature, there are different methods for computing a good regularization parameter, such as the discrepancy principle, the L-curve, and generalized cross validation (GCV) [17].

In this paper, the L-curve method is used for finding a regularization parameter because this method is more visual and can be understood more physically. In the L-curve method for different regularization parameters, the norm of $\left\| I_{reg} \right\|_2$ versus the residual norm of $\left\| E - H \times I_{reg} \right\|_2$ is plotted in a log-log scale as shown in Fig. 3. This plot has always a characteristic of L-shaped appearance and the regularization parameter is determined at the L-curve corner which is corresponds to the minimum of both quantities [17].

III. RESULTS AND DISCUSSION

A. Horn antenna effect of near field distance

In order to evaluate the accuracy of the proposed regularized SRM, first, a horn antenna as shown in Fig. 1, is simulated in a well-known FEM solver HFSS. This horn antenna that is simulated at 2.4 GHz, has a largest dimension of $D=24cm$. Therefore, the RNF region of this antenna extends up to 1.6λ from the antenna aperture. The RNF data of this antenna is obtained in a hemisphere with $0° < \theta < 90°$, $0° < \varphi < 360°$ and angular resolution of $\Delta\theta = 1°$ and $\Delta\varphi = 6°$. The magnetic currents are reconstructed in a rectangular aperture of $40\,cm \times 40\,cm$ with 800 triangular facets and 1160 edges. Therefore, the SRM matrix equation should be solved with 11102 known near field data and 1160 unknown magnetic current coefficients.

For the initial investigation, reactive near field data on a hemisphere with $\lambda/2$ radius from the antenna aperture is used as the input of the proposed regularized SRM. The L-curve plot of this data is shown in Fig. 3.

As it can be seen from this figure, the value of the regularization parameter should be chosen as $\Gamma=0.57$.
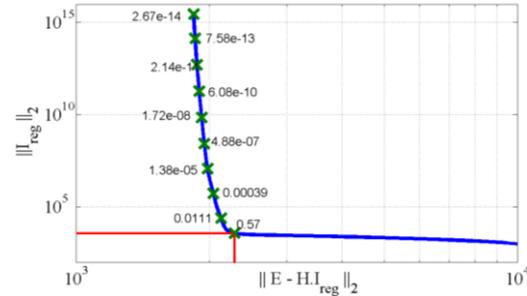
Fig. 3. The L-curve plot of a regularized SRM for $\lambda/2$ reactive near field data of the Horn antenna. The L-curve corner is at $\Gamma= 0.57$.

In order to solve the Tikhonov Equation (6) with this regularization parameter, LSMR solver is used. LSMR is an iterative solver for the least square problem that recently proposed in [18]. In comparison to other iterative solvers like LSQR and CG, the LSMR has better numerical properties and may be able to terminate sooner [18]. The magnetic current that reconstructed by these settings is shown in Fig. 1 (d).

The reconstructed FF pattern of the regularized solver (LSMR with $\Gamma=0.57$) and non-regularized solver (LSMR with $\Gamma=0$) from $\lambda/2$ RNF data are compared with the full wave HFSS simulation in Fig. 4. From this figure, it can be seen that in both E-and H-plane, the regularized algorithm can reconstruct the FF pattern drastically better than the non-regularized solver.
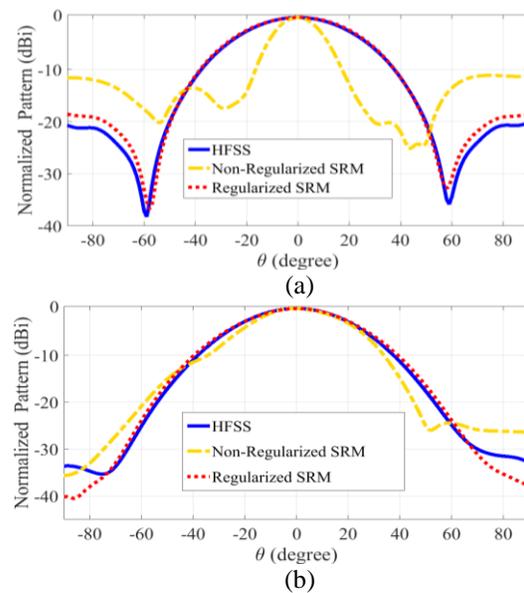
Fig. 4. Comparison of FF pattern of the studied horn antenna in HFSS with the obtained FF pattern of SRM solvers: (a) E-plane and (b) H-plane.

In order to study the necessity of regularization, the FF transformation error (9) of three different near field hemispheres with $\lambda/2$, λ, $3\lambda/2$ radius is evaluated and plotted in Figs. 5 (a), (b) and (c) respectively. The errors are plotted in these figures at each iteration of four different iterative solvers of regularized LSQR, non-regularized LSQR, regularized LSMR and non-regularized LSMR.

(a)

(b)

(c)
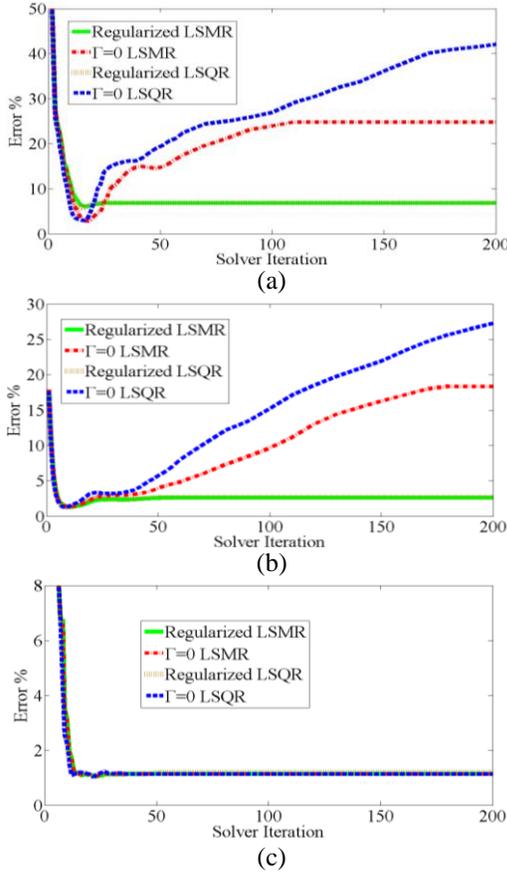
Fig. 5. Comparison of the far field transformation error of regularized and non-regularized solvers in different solver iterations. Input data is a hemisphere with: (a) $\lambda/2$, (b) λ, and (c) $3\lambda/2$, radius.

As it can be seen in these figures, while the regularized solvers have a stable response in all three sub figures, the non-regularized solvers show semi-convergence and instability in Figs. 5 (a) and (b). It should be mentioned that the semi-convergence behavior of the iterative solvers in the presence of noise is already discussed in many publications of regularization [19]. The reason for this behavior is that the early iterations of non-regularized solvers reconstruct correct information about the solution while the later iteration amplifies the noise [19].

In our problem, although noiseless simulation data are used in all three figures, but the evanescent modes in

the reactive near field region of $\lambda/2$ and λ, create such instability in the error plots. As it can be seen in Fig. 5 (c), when these modes are reduced in the $3\lambda/2$ radiative near field region, this instability is also disappeared.

In Fig. 6, the FF transformation error of regularized and non-regularized solvers for near field data of different radii is plotted. As it can be seen in this figure, while in the radiative near field region all methods have almost identical results, in the reactive near field region the non-regularized solvers are oscillating strongly.

Figure 7 shows the value of regularization parameter Γ for the near field data of different radii that calculated by L-curve method. As expected, the value of Γ becomes greater and greater when we approach the antenna aperture, while this value is almost zero in the radiative near field region. In other words, when the evanescent modes are become greater the minimum norm condition ($\left\| I_{reg} \right\|_2$) should be stronger in the least square Equation of (6).

From the above results it can be concluded that while the evanescent modes are part of the input data in the RNF region, they can unstable the SRM field transformation just like a noise signal and a regularization is necessary for the RNF/FF transformation applications.
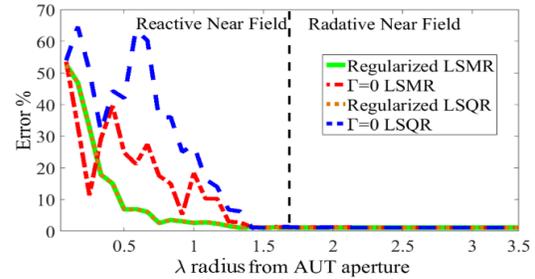
Fig. 6. The far field transformation error of regularized and non-regularized solvers for near field data of different radii.
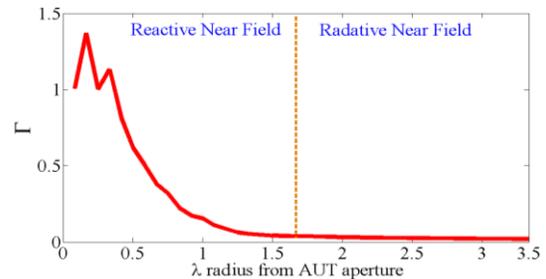
Fig. 7. The value of regularization parameter Γ for the near field data of different radii that calculated by L-curve method.

B. Array antenna effect of SNR

For the second example, consider an array of three

broadband clover leaf dipole antenna as shown in Fig. 8. Clover leaf antennas are originally a broadband cross dipole antennas and are frequently used in base transceiver station (BTS) structures [20]. This antenna is simulated in 1.7 GHz frequency in a well-known FDTD solver CST.
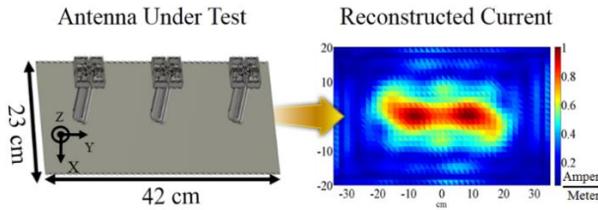
Fig. 8. The configuration of four leaf array antenna and the equivalent magnetic current that reconstructed by the regularized SRM from RNF data of 1.3λ.

The largest dimension of this antenna is equal to 48 cm, therefore, the RNF region of this antenna extends up to *2.8λ* from the antenna aperture. The near field data of this antenna is obtained in a hemisphere with $0° < \theta < 90°$, $0° < \varphi < 360°$ and angular resolution of $\Delta\theta = 4°$ and $\Delta\varphi = 3°$. The magnetic currents are reconstructed by SRM in a rectangular aperture of *70 cm ×40 cm* and this aperture is meshed with 2000 triangular facets and 2935 edges. Therefore, the SRM matrix equation should be solved with 5566 known near field data and 2935 unknown magnetic current coefficients.

The reconstructed magnetic current of the regularized LSMR solver from the RNF data of a hemisphere with *1.3λ* radius is shown in Fig. 8. The FF pattern that reconstructed by the regularized and non-regularized LSMR are compared with the full wave CST simulation results in Fig. 9. As it can be seen in the both E- and H-planes, the regularized SRM are again reconstructed the FF pattern more accurate than the non-regularized ones. It should be mentioned that a little deviation that can be seen in the calculated pattern of regularized SRM over the horizon angles are mainly due to the truncation error in the reconstructed equivalent current domain as described in [7]. Theoretically, it is assumed that magnetic currents are reconstructed in an infinite surface; however, in the practical computation this surface is truncated at a specified distance. The other important reason is considering only the currents of antenna aperture in SRM calculation while in the full wave simulation scattering from the antenna body is also considered. Therefore calculated pattern with SRM is valid at angles above the horizon [7].

For this example, we try to show the effectiveness of the regularized SRM in the presence of noise. Therefore, a Gaussian noise with different SNR is added to the reactive near field data of CST software. The far field transformation error of non-regularized and regularized LSMR for near field data of different radii in different SNRs is plotted in Figs. 10 (a) and (b), respectively. As it can be seen in this figure, the regularized SRM have more accurate results in all cases especially in the RNF region (less than *2.8λ*). It also can be seen that in the radiative near field region the regularization reduce the effect of Gaussian noise when the SNR is not so high.

From these results, it can be understood that in the RNF region due to the presence of a large amount of evanescent modes a regularized SRM should be used instead of the conventional SRM. It is shown that the regularized SRM in RNF/FF application can create more stable and accurate transformation whether RNF data are noiseless or noisy.
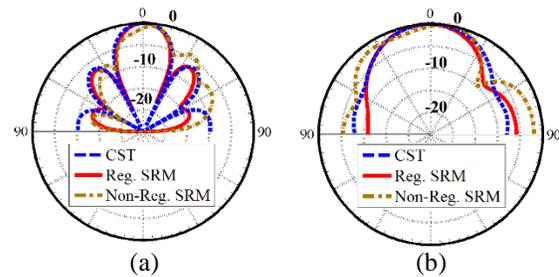
Fig. 9. Comparison of FF pattern of the four leaf antenna in CST with the obtained far field pattern of a regularized and non-regularized SRM from RNF data of 1.3λ: (a) E-plane and (b) H-plane.
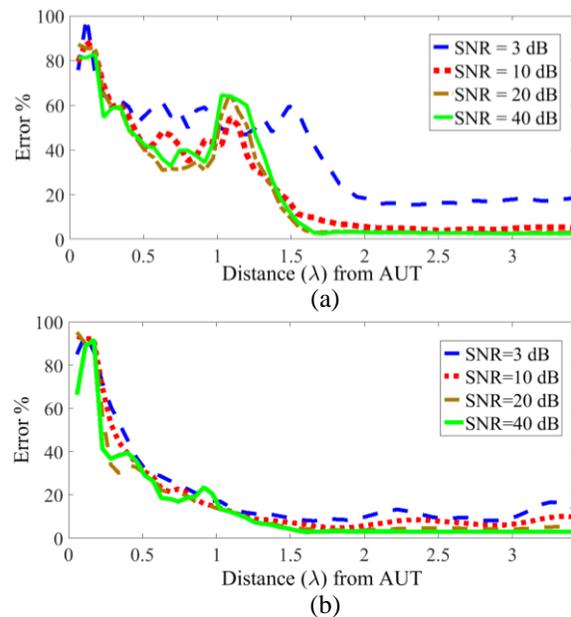
Fig. 10. The far field transformation error of LSMR solver for near field data of different radii in different SNRs: (a) non-regularized LSMR solver, and (b) regularized LSMR solver.

VI. CONCLUSION

In this paper, the RNF/FF transformation based on the SRM technique has been studied carefully. It has been shown that in the RNF region whether the input data is noisy or noiseless, the evanescent modes can unstable the SRM iterative solvers. It has been shown analytically that the RNF instability can be resolved by using a Tikhonov SRM equation. The regularization parameter of the Tikhonov equation has been determined by the well-known L-curve method. In order to evaluate the accuracy of the proposed regularized SRM two different antenna with different conditions has been simulated. Far field transformation error of theses antennas has been evaluated by both regularized and non-regularized solvers. It has been shown that in the RNF region the non-regularized SRM is unstable and failed to reconstruct the correct pattern, while the regularized SRM is maintained stable and can create better transformation both in the presence and non-presence of Gaussian noise. According to the results of this paper, a regularized SRM should be used instead of conventional SRM for the RNF/FF applications.

REFERENCES

[1] A. Yaghjian, "An overview of near-field antenna measurements," *IEEE Trans. Antennas Propag.*, vol. 34, pp. 30-45, Jan. 1986.

[2] L. Zhiping, Z. Wang, and W. Jianhua, "Computer reconstructed holographic technique for phase-less near-field measurement," *ACES Journal*, vol. 28, no. 12, pp. 1199-1204, Dec. 2013.

[3] Y. Alvarez, F. Las-Heras, and M. R. Pino, "On the comparison between the spherical wave expansion and the sources reconstruction method," *IEEE Trans. Antennas Propag.*, vol. 56, no. 10, pp. 3337-3341, Oct. 2008.

[4] A. Taaghol and T. K. Sarkar, "Near-field to near/far-field transformation for arbitrary near-field geometry, utilizing an equivalent magnetic current," *IEEE Trans. on Elec. Comp.*, vol. 38, no. 3, pp. 536-542, Aug. 1996.

[5] T. K. Sarkar and A. Taaghol, "Near-field to near/far-field transformation for arbitrary near-field geometry utilizing an equivalent electric current and MoM," *IEEE Trans. Antennas Propag.*, vol. 47, no. 3, pp. 566-573, Mar. 1999.

[6] J. Colinas, Y. Goussard, and J. J. Laurin, "Application of the Tikhonov regularization technique to the equivalent magnetic currents near-field technique," *IEEE Trans. Antennas Propag.*, vol. 52, no. 11, pp. 3122-3132, Nov. 2004.

[7] F. Las-Heras, M. R. Pino, S. Loredo, Y. Alvarez, and T. K. Sarkar, "Evaluating near-field radiation patterns of commercial antennas," *IEEE Trans. Antennas Propag.*, vol. 54, no. 8, pp. 2198-2207, Aug. 2006.

[8] Y. Alvarez, F. Las-Heras, and M. R. Pino, "Reconstruction of equivalent currents distribution over arbitrary three-dimensional surfaces based on integral equation algorithms," *IEEE Trans. Antennas Propag.*, vol. 55, no. 12, pp. 3460-3468, Dec. 2007.

[9] Y. Alvarez Lopez, F. Las-Heras Andres, M. R. Pino, and T. K. Sarkar, "An improved super-resolution source reconstruction method," *IEEE Trans. Instrum Meas.*, vol. 58, no. 11, pp. 3855-3866, Nov. 2009.

[10] C. H. Schmidt and T. F. Eibert, "Integral equation methods for near-field far-field transformation," *ACES Journal*, vol. 25, no. 1, pp. 15-22, Jan. 2010.

[11] J. L. Araque Quijano and G. Vecchi, "Improved-accuracy source reconstruction on arbitrary 3-D surfaces," *IEEE Antennas Wireless Propag. Lett.*, vol. 8, pp. 1046-1049, 2009.

[12] J. L. Araque Quijano and G. Vecchi, "Near- and very near-field accuracy in 3-D source reconstruction," in *IEEE Antennas Wireless Propag. Lett*, vol. 9, pp. 634-637, 2010.

[13] P. Vinetti, *A Non-Invasive, Near-Field and Very Near-Field Phaseless Antenna Characterization System*, Ph.D. dissertation, Universita di Napoli Federico II, Nov. 2008. (Available at http://www.fedoatd.unina.it/1343/2/Tesi_Dottorato_PV_v2.pdf)

[14] A. Capozzoli, et al., "Dielectric field probes for very-near-field and compact-near-field antenna characterization [measurements corner]," *IEEE Antennas Propag. Mag.*, vol. 51, no. 5, pp. 118-125, Oct. 2009.

[15] D. J. Lee, J. Y. Kwon, N. W. Kang, J. G. Lee, and J. F. Whitaker, "Vector-stabilized reactive-near-field imaging system," *IEEE Trans. Instrum. Meas.*, vol. 60, no. 7, pp. 2702-2708, July 2011.

[16] M. E. Kilmer and D. P. O'Leary, "Choosing regularization parameters in iterative methods for ill-posed problems," *SIAM J. Matrix Anal. Applicat.*, vol. 22, no. 4, pp. 1204-1221, 2001.

[17] P. C. Hansen, "Rank-deficient and discrete ill-posed problems: Numerical aspects of linear inversion," *SIAM*, vol. 4, 1998.

[18] D. C.-L. Fong and M. A. Saunders, "LSMR: An iterative algorithm for sparse least-squares problems," *SIAM J. Sci. Comput.*, vol. 33, no. 5, pp. 2950-2971, Oct. 2011.

[19] J. Chung, J. G. Nagy, and D. P. O'Leary, "A weighted GCV method for Lanczos hybrid regularization," *Electron. Trans. Numerical Anal.*, vol. 28, pp. 149-167, Jan. 2008.

[20] G. M. Lytle, J. L. Schadler, and D. Kokotoff, "*Broadband Clover Leaf Dipole Panel Antenna*," U.S. Patent 8 558 747, Oct. 15, 2013.